
Article:
Dost, R. orcid.org/0000-0002-8578-0389, Zhou, Y., Zhang, H. et al. (2 more authors) (2020) Effect of annealing on the electrical and magnetic properties of electrodeposited Ni and permalloy nanowires. Journal of Magnetism and Magnetic Materials, 499. 166276. ISSN 0304-8853

https://doi.org/10.1016/j.jmmm.2019.166276

Effect of annealing on the electrical and magnetic properties of electrodeposited Ni and Permalloy nanowires

R Dost[1,*], Y Zhou[2], H Zhang[2], D A Allwood[1] and B J Inkson[1]

[1] Dept. of Materials Science & Engineering, University of Sheffield, Sheffield, UK
[2] CRANN – AML, Trinity College Dublin, Dublin, Republic of Ireland

Abstract. The influence of annealing on the microstructure and the electrical and magnetic properties of cylindrical nickel-based nanowires has been investigated. Nanowires of nickel of ~275 nm diameter and of permalloy (Py) of ~70 nm diameter were fabricated by electrochemical deposition into nanoporous templates of polycarbonate and anodic alumina, respectively. Characterization was carried out on as-grown and up to 650 °C heat-treated nanowires. Transmission electron microscopy imaging and diffraction of the nanowires showed a temperature-correlated grain growth of an initially nanocrystalline structure (untreated) with <8 nm (Ni) and <20 nm (Py) grains towards coarser poly-crystallinity after heat treatment with grains up to ~160 nm (Ni) and ~70 nm (Py), the latter being limited by the nanowire width. The electrical conductivity of individual as-grown and 650 °C annealed Ni nanowires was measured in-situ by scanning electron microscopy. At low current densities, the conductivity of annealed nanowires was estimated to have doubled over as-grown nanowires. We attribute this increase to the observed grain growth. The annealed nanowire was subsequently subjected to increasing current densities. Above 120 kA.mm^{-2} the nanowire resistance started to rise. At 450 kA.mm^{-2}, the nanowire melted and current flow ceased. Magnetometry of as-grown and annealed nanowire arrays showed them to display quasi-thin film magnetic properties. Coercivity and saturation field were inversely correlated in annealed wires and a 25% tunability in these properties was achieved at just 200 °C.

1. Introduction

In 1995 Masuda *et al*. demonstrated the controlled fabrication of nanoporous anodic alumina (AAO) templates [1], enabling the subsequent fast and reliable growth of electrodeposited metallic nanowires. Variations of this approach have developed to allow growth of complex nanowires, including modulated composition [2, 3] and defined shape [4]. Electrodeposited nanowires of ferromagnetic materials are of interest due to their promise for applications in such as high-frequency devices [5], high-density magnetic recording [6], sensors [7], biomedicine [8] and spintronic devices [9, 10]. Cylindrical nanowires are particularly attractive due to their axial symmetry and tunable shape anisotropy [11, 12]. A range of magnetic nanowires has been successfully fabricated by AAO, with nickel-based nanowires demonstrating excellent magnetic properties, e.g. [13, 14].

The structural [15], magnetic [2, 16] and electrical properties [3, 17] of cylindrical magnetic nanowires require detailed characterization, which requires overcoming challenges arising from their small size, fragility and particular features such as small magnetic volume, large shape anisotropy, and magnetostatic coupling (when in array conformation). Here we assess the effect of heat treatment on the grain size of nickel-based cylindrical nanowires and on their electrical and magnetic properties for controlling their functional properties as magnetic transducers.

* Corresponding author. *E-mail:* r.dost@sheffield.ac.uk

https://doi.org/10.1016/j.jmmm.2019.166276
Available online 11 December 2019

2. Sample preparation

A nanoporous AAO template with about 65–75 nm pore diameter and 20 nm pore spacing was prepared from a 100 µm thick aluminium sheet (Goodfellow®, 99.99% pure). The aluminium was first polished in an electrochemical cell with 1:4 parts solution of perchloric acid and ethanol at DC currents of 2–3 A, then mild anodized in an aqueous solution of 0.3 mol/l oxalic acid and 0.05 mol/l phosphoric acid at 33 V for 3 h. The AAO layer was then separated with mercury(II) chloride, and the barrier layer was removed in 0.5 mol/l phosphoric acid for 90 min. The used electrolyte chemistries are based on our previous work [3, 10]. A VoltaLab® PGZ 402 voltammetry cell was used for the electrochemical deposition of nickel and permalloy ($Ni_{80}Fe_{20}$; Py) nanowires into nanoporous templates at a DC potential of −1.2 V for 45 min. Cylindrical Py nanowires of ~70 nm diameter were electrodeposited in the AAO template from a solution containing 90 g/l $NiSO_4$, 13.5 g/l $FeSO_4$, 30 g/l H_3BO_3 as a pH buffer and 5 g/l L-ascorbic acid as antioxidant. The Py nanowires typically grew to be 6 µm long with an aspect ratio of ~85. Cylindrical Ni nanowires of ~275 nm diameter were, however, electrodeposited in a commercially available nanoporous polycarbonate (PC) template (Whatman® Nuclepore 111106, 0.2 µm) from a solution containing 90 g/l $NiSO_4$, 30 g/l H_3BO_3, 5 g/l L-ascorbic acid and 1 wt% gelatine as hydrophilic agent. The Ni nanowires typically grew to be 9 µm long with an aspect ratio of ~33.

Fabricated nanowires were characterized by scanning electron microscopy (SEM; FEI Nova™ NanoSEM 450), He-ion microscopy (HIM; Carl Zeiss ORION® PLUS) and transmission electron microscopy (TEM; JEOL JEM 3010). Figure 1(a) shows the nanoporous structure of a typical grown AAO template with parallel nanopores of diameter ~70 nm separated by 20nm thick alumina walls. The Py nanowires electrodeposited into these templates were typically 6 µm long (Fig. 1(b)), dependent on plating parameters and electrical connection to individual pores.

While still in their template, Py and Ni nanowires were subjected to heat treatment in a furnace under a protective N_2 atmosphere. Temperatures were raised to either 200 °C, 400 °C or 650 °C and held for 1 hr. The furnace was then allowed to naturally cool down before the templates were removed. We refer to the untreated nanowires as *as-grown* and the heat-treated nanowires as *annealed*. For microstructural analysis, some as-grown and annealed Ni and Py nanowires were released by dissolving their templates in chloroform and 1M NaOH solution, respectively, and drop cast from suspension onto silicon substrates. Nanowires dispersed randomly and came to rest either isolated or in bundles (Fig. 1(c)).

SQUID (superconducting quantum interference device) magnetometry was performed at 300 K using a Quantum Design MPMS 2.1. Magneto-optical Kerr effect (MOKE) magnetometry was performed using a custom-built instrument that used 632 nm wavelength light from a laser diode producing 3 mW output power. Measurements were conducted in the polar MOKE configuration [18] with near-normal incident light to ensure sensitivity to out-of-plane sample magnetization. MOKE data from 64 field cycles were averaged to produce a single hysteresis loop.

The nanowires were electrically probed inside a SEM environment by two Kleindiek MM3A-EM micromanipulators fitted with sharp tungsten probes (Fig. 1(c) Inset). All electrical measurements used the same pair of W-probes with a measured tip-to-tip resistance (R_t) of ~30 Ω. To make good mechanical contact with the nanowires, the tungsten tips applied a gentle vertical pressure. To make good electrical contact, i.e. minimising the effect of contact resistance (R_c), current-voltage (*I-V*) measurements were preceded by one or more 'burn-in' bias sweeps of varying magnitude (initially at $\pm$0.1V, if necessary rising to $\pm$1V or more). In the case that contamination or oxides may have been present on the nanowire surface, this process would cause dielectric breakdown. The threshold field for NiO is in the range of $0.6\ldots9\times10^8$ V/m and characterised by a substantially reduced NiO resistance of at least five orders of magnitude [19, 20]. Indeed, the total resistance $R = R_c + R_t + R_{nw}$, where R_{nw} is the resistance of the actual nanowire, dropped from an initial order of kΩ–MΩ down to typically <100 Ω until it dropped no further for successive bias sweeps. A number of burnt-in nanowires of the same heat treatment and length (i.e. probe spacing) had their total resistances settle around the same minimum value with about ±2% variability.

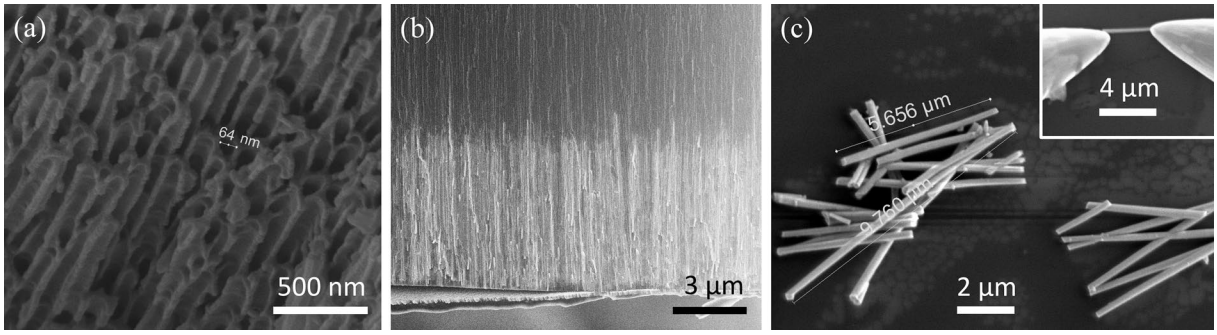

Figure 1. (a) SEM image of a fractured nanoporous AAO template. (b) HIM image of permalloy nanowires electro-deposited into an AAO template. The permalloy nanowires (bright contrast) are visible extending ~6 µm into the pores (dark contrast). (c) Randomly oriented as-grown Ni nanowires after drop casting from a chloroform suspension. Inset: tungsten tips making electric contact with a single Ni nanowire.

3. Experimental results

3.1. Nanowire Microstructure

TEM imaging and diffraction was used to characterize the grain sizes of as-grown and annealed nanowires. The as-grown nanowires were nanocrystalline with grain sizes of Py <20 nm (Fig. 2(a)) and Ni <8 nm (Fig. 3(a)). The Py nanowires exhibited occasional bumps from AAO pore irregularities and small surface aggregates of undissolved alumina template (Fig. 2), making them more irregular in shape. When occasional nanowire branching occurred (Fig. 2(a)), their diameters might vary by up to ±20% across their full length. In comparison, the as-grown PC-templated Ni nanowires were much smoother (Fig 3(a)) and exhibited a slight spindle-shape due to the track-etched PC template geometry [21].

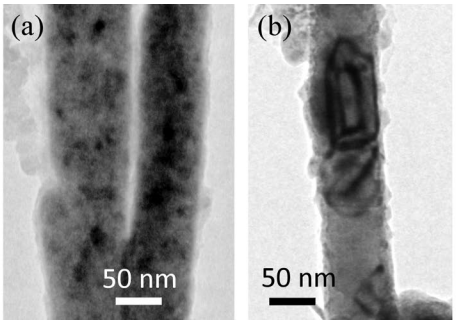

Figure 2. TEM images of 75 nm wide Py nanowires. (a) Two as-grown nanowires with grain sizes ≤20 nm. (b) After annealing at 650 °C, grains had grown to the full nanowire width.

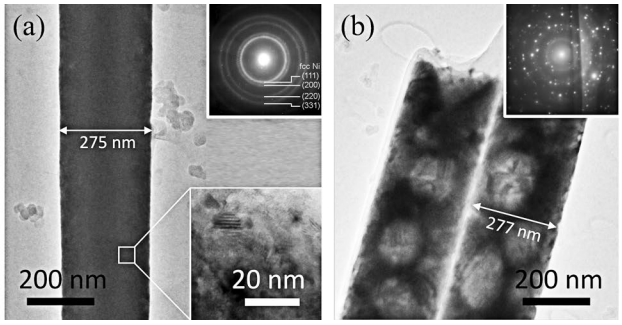

Figure 3. TEM images of 275 nm wide Ni nanowires. (a) Before annealing grain sizes are ≤8 nm (see magnified area). (b) After annealing at 650 °C, grain sizes are up to ~160 nm. Insets: Representative diffraction patterns.

Heat treatment of the templated nanowires induced grain growth in both the Py and Ni nanowires. After 1h annealing at 650 °C, the Py nanowires featured large grains that in some cases spanned the entire nanowire width (~70 nm), forming a near 'bamboo structure' (Fig. 2(b)) [22]. The thicker polycrystalline Ni nanowires (~275 nm) also exhibited grain coarsening, growing grains up to 160 nm (Fig. 3(b)). There was insignificant grain growth at 200 °C and 400 °C (not shown here), and the onset of pronounced grain growth was thus raised by at least 200 K compared to pure Ni films [23]. Grain growth did not result in changes to Py or Ni nanowire diameter (to within ~2%, which might well represent intrinsic template pore-to-pore variations), observed by comparing average diameters of

randomly chosen as-grown and annealed nanowires. The presence of nickel oxides, which can arise from annealing Ni nanowires in air/O_2 [24], was not observed here, with annealing conducted in a protective N_2 atmosphere.

3.2. Nanowire Electrical Properties

To quantify the influence of grain-size on electrical properties, the electrical conductivities of as-grown and 650 °C heat-treated individual Ni nanowires (275 nm diameter) were determined from current-voltage (*I-V*) measurements of known lengths (L) of nanowire. Not further discussed are measurements on 200 °C annealed nanowires, which showed little to no change compared with as-grown samples, likely due to the unchanged microstructure. For the calculations, all nanowire diameters were assumed identical (see above). Electrical measurements of Py nanowires were not possible due to their much smaller diameter compared with the Ni nanowires.

Figure 4(a) shows the *I-V* curve of an as-grown nanocrystalline Ni nanowire at ±0.1 V forward-reverse bias and 2.6 μm probe spacing ($L^{(a)}$). The as-grown nanowire exhibits a linear *I-V* characteristic within the applied ±0.1 V sweep, with a maximum current density ($J^{(a)}$) of 43 kA.mm^{-2} and a resistance $R^{(a)} = 38.7\ \Omega$. Figure 4(b) shows the *I-V* curve of a 650 °C annealed nanowire at up to 1.5 V forward-bias and 2.9 μm probe spacing ($L^{(b)}$). The bias was deliberately increased to show the nanowire electrical behaviour beyond its low-bias regime. The 650 °C annealed nanowire exhibited four distinct regimes during the high voltage sweep (see ①–④ in Fig. 4(b)). At low bias <0.26 V corresponding to $J^{(b)} = 0$–120 kA.mm^{-2}, the annealed nanowire electrical behaviour was Ohmic with total resistance $R^{(b)} = 34.9\ \Omega$. At increased bias 0.26–0.60 V equal to $J^{(b)} = 120$–240 kA.mm^{-2}, $R^{(b)}$ jumped to 51.7 Ω, likely due to Joule heating. Above 0.6 V where $J^{(b)} > 240$ kA.mm^{-2}, $R^{(b)}$ fluctuated erratically, likely due to metal diffusion and nanowire shape change driven by Joule heating. Current flow abruptly ceased at $J^{(b)} = 450$ kA.mm^{-2}. As confirmed *in-situ* during SEM imaging, the nanowire melted from excessive Joule heating.

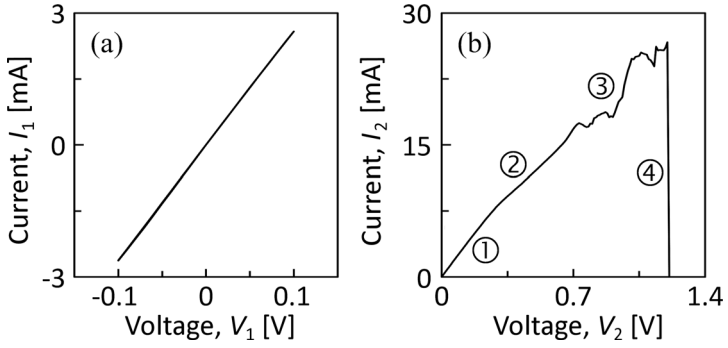

Figure 4. (a) *I-V* characteristic (±0.1V) of an individual as-grown Ni nanowire (diameter = 275 nm, length = 2.6 μm). (b) *I-V* characteristic (0-1.5V) of an individual Ni nanowire annealed at 650 °C (diameter = 275 nm, length = 2.9 μm).

The change in conductivity between as-grown ($\sigma_{nw}^{(a)}$) and annealed ($\sigma_{nw}^{(b)}$) nanowires was estimated for unknown contact resistances $R_c^{(a)}$, $R_c^{(b)}$ by evaluating both *I-V* curves in the low biasing linear regime at identical currents of $I^{(a)} = I^{(b)} = 2.58$ mA (arbitrary). The corresponding voltages were $V^{(a)} = 99.90$ mV and $V^{(b)} = 90.01$ mV. Given that $V/I = R$, we thus observed a ~10% drop in total resistance ($R^{(b)}/R^{(a)} - 1$).

Nanowire conductivity is given by $\sigma_{\mathrm{nw}} = L(AR_{\mathrm{nw}})^{-1}$. Given the same nanowire cross-sectional areas A (with constant diameters of 275 nm) but accounting for different probe spacings ($L^{(\mathrm{a})}$, $L^{(\mathrm{b})}$), the conductivity ratio for annealed to as-grown nanowires is

$$\frac{\sigma_{\mathrm{nw}}^{(\mathrm{b})}}{\sigma_{\mathrm{nw}}^{(\mathrm{a})}} = \frac{L^{(\mathrm{b})}}{L^{(\mathrm{a})}} \times \frac{R^{(\mathrm{a})} - R_{\mathrm{c}}^{(\mathrm{a})} - R_{\mathrm{t}}}{R^{(\mathrm{b})} - R_{\mathrm{c}}^{(\mathrm{b})} - R_{\mathrm{t}}} \tag{1}$$

We need to consider the realistic values of the contact resistances in order to be able to comment on the likely changes in nanowire conductivity. We may assume that nanowires of the same type, history and length will exhibit roughly the same intrinsic nanowire resistance ($R_{\mathrm{nw}} \cong$ const). The measured post burn-in consistency in R with about ±2% variability, together with the assumed invariabilities in R_{t} and R_{nw}, imply that the variability in R_{c} should itself be limited to about ±0.02 R for a given nanowire. That is, $\Delta R_{\mathrm{c}}^{(\mathrm{a})} \approx \pm 0.77\ \Omega$ and $\Delta R_{\mathrm{c}}^{(\mathrm{b})} \approx \pm 0.70\ \Omega$. Since we were unable to vary the contact spacing on individual nanowires we could not measure contact resistances directly. However, an estimate for R_{c} must not exceed a value that is limited by the conductance of the nanowires, which itself is limited by that of high purity Ni, $\sigma_{\mathrm{bulk}} = 1.43\times10^{7}$ S.m^{-1} [25]. That is, substituting the nanowire conductivity in $R_{\mathrm{c}} = R - R_{\mathrm{t}} - L(A\sigma_{\mathrm{nw}})^{-1}$ with σ_{bulk} provides upper limits for $R_{\mathrm{c}}^{(\mathrm{a})} = 5.66\ \Omega$ and $R_{\mathrm{c}}^{(\mathrm{b})} = 1.47\ \Omega$. The similarities in geometry and material between as-grown and annealed nanowire and the improbability that the annealing step reduced contact resistance (on the nanowire surface) mean we shall assume contact resistances for the two cases are bound by the smaller of the two limits calculated. Hence, the upper limit of $R_{\mathrm{c}}^{(\mathrm{a})}$ reduces to about 1.47 Ω, or less. The likely magnitudes for the unknown contact resistances are thus $R_{\mathrm{c}}^{(\mathrm{a})} \leq R_{\mathrm{c}}^{(\mathrm{b})} \approx (0.73\pm0.73)\ \Omega$, which are compatible with above estimates of their variabilities. In comparison, the drop in total resistance for the annealed nanowire over the as-grown one was measured at $R^{(\mathrm{b})} - R^{(\mathrm{a})} = 3.8\ \Omega$. We therefore argue that this magnitude of resistance drop cannot be solely attributed to different and unknown contact resistances between measurements (a) and (b) alone. The change in measured resistance is likely to have also resulted from a reduction in R_{nw} when nanowires were annealed. With Eq. 1, the resultant relative change in nanowire conductivity $\sigma_{\mathrm{nw2}}/\sigma_{\mathrm{nw1}}$ amounts to anywhere from about 2.0 to 2.8, with the lower limit set by $R_{\mathrm{c}}^{(\mathrm{a})} = R_{\mathrm{c}}^{(\mathrm{b})} \to 0$ and the upper limit given by $R_{\mathrm{c}}^{(\mathrm{a})} \sim 0$, $R_{\mathrm{c}}^{(\mathrm{b})} = 1.47\ \Omega$. This range is narrowed further to about 2.0–2.4 under the assumption that $R_{\mathrm{c}}^{(\mathrm{a})} \cong R_{\mathrm{c}}^{(\mathrm{b})}$. Assuming the physically most plausible values for the unknown contact resistances, $R_{\mathrm{c}}^{(\mathrm{a})} \sim R_{\mathrm{c}}^{(\mathrm{b})} > 0$, we conclude the nanowire conductivity must have increased by a little over factor two to explain the observed drop in total resistance.

The observed increase in electrical conductivity in Ni nanowires undergoing annealing is most likely due to the grain growth observed in Figures 2 and 3. Larger grains mean fewer grain boundaries, which are sites of increased electron scattering and which contribute to electrical resistance. In addition, it is likely that the grain growth is accompanied by reduced dislocation density and release of microstrains [26].

3.3. Nanowire Magnetic Properties

SQUID magnetometry was performed on arrays of Ni and Py nanowires still in their templates, with magnetisation measured along the nanowires' long axis. The hysteresis loops of Py, as-grown and annealed, are shown in Figure 5(a) (black plots), and of as-grown Ni in Figure 5(b). All nanowires exhibited ferromagnetic properties. Additionally, MOKE magnetometry was used to measure the as-grown Py nanowire array, after the AAO template had been surface-polished with a 1 μm grid diamond film (grinder: Minimet 1000, force: 13.4 N, time: 9 minutes) and with magnetic field applied normal to the template surface and parallel to the nanowires' long axis. Despite its surface sensitivity, the MOKE measurements are likely to be highly representative of the nanowires' behaviour as a whole. Soft-magnetic cylindrical wires are known to reverse magnetisation via domain wall nucleation at a wire end followed by its rapid propagation through the wire [27]. The data, overlaid in Figure 5(a) (red plot), agree well with the SQUID data in terms of saturation field and overall loop shape. All the measurements

of in-template nanowire arrays showed low remanence, which we attribute to magneto-static interactions between wire ends [28]. Due to the inter-pore distances of the templates (approx. 20 nm for AAO) and the nanowire lengths, the nanowire arrays may have acted as quasi-thin films with an in-plane easy axis and out-of-plane hard axis [13]. The as-grown Py array had a saturation magnetic field (H_S) of approximately 240 kA.m^{-1} (MOKE) to 270 kA.m^{-1} (SQUID). H_S of the annealed Py arrays remained close to the as-grown value with the exception of the 400 °C sample, for which H_S = 240 kA m^{-1} (Fig. 5 (c); black squares). We consider the saturation field to be largely unaffected by the heat-treatment and ascribe the observed dip at 400 °C to experimental errors. H_S of the as-grown Ni array was about 72 kA.m^{-1}. This lower saturation field is consistent with a weaker quasi-thin film behaviour due to a larger template inter-pore spacing and lower magnetization of Ni compared with Py. This is supported by studies for up to 500 nm pore distance [29]. The Ni templates did not survive annealing so magnetometry was not possible for heat-treated Ni wires.

The MOKE measurement required the top surface of the slightly warped Py template to be ground flat and polished, which significantly reduced the template thickness and, thus, the lengths of the embedded nanowires. Because of this, the coercivity of MOKE measurements was typically about half that of similar SQUID measurements for the as-grown Py array (Fig. 5(c)). Our as-grown Py nanowire coercivity of H_C = 40 kA.m^{-1} compares with 59 kA.m^{-1} published for a Py nanowire array in template with an identical 70 nm nanowire diameter [14], and 52 kA.m^{-1} for a micromagnetic simulation of a polycrystalline Py nanowire with 70 nm diameter [30]. Different electrodeposition parameters and pore distances (not specified) are likely to account for the slight differences in values across these studies. The coercivity of the Py nanowire arrays has a marked 25% dip to 29 kA.m^{-1} at 200 °C and recovers for higher annealing temperatures to the as-grown value of 40 kA.m^{-1} (Fig. 5(c); black circles). Such a coercivity dip was reported at similar temperatures for as-deposited and annealed Ni/Ni-alloyed films [23]. We explain the observed H_C variations here with temperature-dependent dislocation densities. Crystal imperfections act as domain wall pinning sites, elevating the coercivity. When lower temperature annealing is applied, those imperfections are relieved, minimising the coercivity at or around 200 °C. For higher annealing temperatures, coercivity rises again as nanocrystals grow.

Our as-grown Ni sample had H_C = 10 kA.m^{-1}. This is lower than for the Py samples, which is explained by the larger diameter of Ni wires, and comparable to that of studies of similar samples [29].

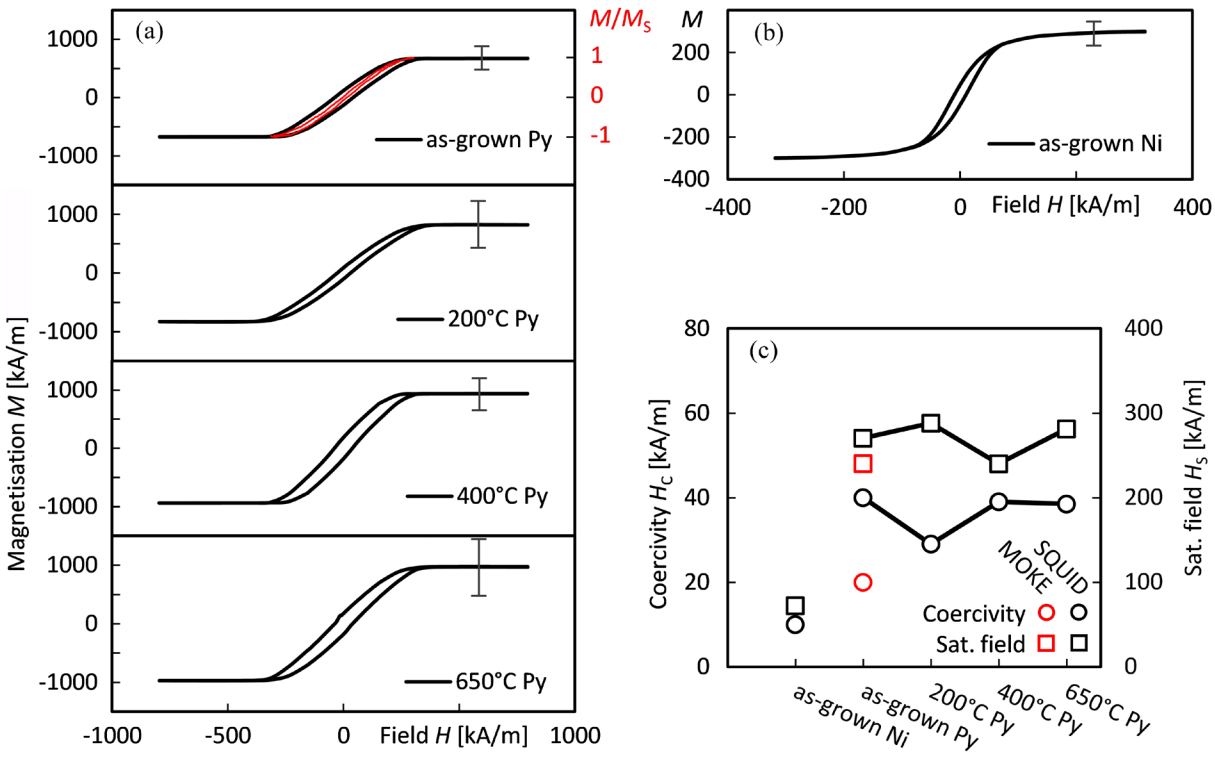

Figure 5. SQUID (black) and polar-MOKE (red) measurements of (a) permalloy nanowire arrays (∅70 nm) in AAO template (corrected for diamagnetism of AAO template), and (b) of a nickel nanowire array (∅275 nm) in PC template. The grey curves indicate the uncertainty in M as a direct result of the error in permalloy/nickel volume estimates, which was limited by a balance resolution of 0.01 mg. (c) Coercivities (H_C) and saturation fields (H_S) of all nanowire arrays, deduced from the Squid (black) and MOKE (red) measurements.

4. Conclusion

We have shown that the grain structure of magnetic cylindrical nanowires can be altered through heat treatment, which causes significant grain growth, tending towards a bamboo-type microstructure. This in turn reduces the grain boundary surface area with an approximately two-fold increase in electrical conductivity for the 650 °C annealed nickel nanowires. Current densities above about 120 kA.mm^{-2} lead to Joule heating and degrade conductivity until structural failure. Magnetic properties of the nanowire arrays display quasi-thin film characteristics. Saturation magnetization appears robust against heat-treatment within experimental uncertainty. Saturation field remains largely robust against heat-treatment, with one 11% deviation from this attributed to experimental error. Coercivities of as-grown Ni and Py nanowires are comparable to those from previous studies while the heat-treated Py nanowires offer some tunability of coercivity, each of about 25% between as-grown and 200 °C, possibly due to annealing of defects up to 200 °C, and grain growth from 400 °C.

Declaration of Competing Interest

The authors declare that they have no known competing financial interests or personal relationships that could have appeared to influence the work reported in this paper.

Acknowledgement

This work was supported by the Engineering and Physical Sciences Research Council (grant number EP/L020696/1).

References

[1] H Masuda and K Fukuda 1995 *Science* **268** 1466–8
[2] K O Moura *et al*. 2016 *Sci. Rep.* **6** 28364
[3] M Elawayeb *et al*. 2012 *J. Appl. Phys.* **111** 034306
[4] W Lee, R Ji, U Gösele and K Nielsch 2006 *Nat. Mater.* **5** 741–7
[5] J C Frake *et al*. 2015 *Sci. Rep.* **5** 1–6
[6] M I Irshad, F Ahmad and N M Mohamed 2012 *AIP Conf. Proc.* (Malaysia. Melville: AIP) 625
[7] X Chena *et al*. 2013 *Sensor Actuat.* B: Chem. **177** 178–95
[8] F Patolsky, G Zheng and C M Lieber 2006 *Nanomedicine* **1** 51–65
[9] F Ciubotaru 2012 Thesis: *Spin-wave excitation by nano-sized antennas* (University of Kaiserslautern)
[10] M Elawayeb, Y Peng and B J Inkson 2011 *J. Nanosci. Nanotechnol.* **11** 7777–82
[11] V V Kruglyak, S O Demokritov and D Grundler 2010 *J. Phys.* D: Appl. Phys. **43** 264001
[12] B Lenk *et al*. 2011 *Phys. Rep.* **507** 107–36
[13] M S Salem and K Nielsch 2017 *Mat. Sci. Eng. B* **223** 120–4
[14] M S Salem *et al*. 2012 *J. Mater. Chem.* **22** 8549–57
[15] K Maaz *et al*. 2010 *Nanoscale Res. Lett.* **5** 1111–17
[16] A Encinas-Oropesa, M Demand and L Piraux 2001 *Phys. Rev. B* **63** 104415
[17] J Wu *et al*. 2014 *Appl. Phys. Lett.* **105** 183506
[18] A Hubert and R Schaefer 1998 *Magnetic Domains: The Analysis of Magnetic Microstructures* Springer-Verlag Berlin Heidelberg ISBN: 978-3-540-64108-7
[19] S Krishnan, E Stefanakos and S Bhansali 2008 *Thin Solid Films* **516** 2244–50
[20] N Fuschillo, B Lalevic and B Leung 1974 *Thin Solid Films* **24** 181–92
[21] C Schönenberger *et al*. 1997 *J. Phys. Chem. B* **101** 5497–505
[22] M Hummelgård *et al*. 2010 *Nanotechnology* **21** 165704
[23] E Pellicer *et al*. 2011 *ACS Appl. Mater. Interfaces* **3** 2265–74
[24] S Han 2007 *Mater. Lett.* **61** 1105–8
[25] M J Laubitz, T Matsumura and P J Kelly 1976 *Can. J. Phys.* **54** 92–102
[26] R E Reed-Hill 2009 *Physical Metallurgy Principles*, *4th ed.* Stamford: Cengage Learning ISBN: 0-495-08254-6
[27] R Hertel and J Kirschner 2004 *J. Magn. Magn. Mater.* **278** L292–7
[28] S Goolaup *et al.* 2007 *Phys. Rev. B* **75** 144430
[29] J Escrig *et al*. 2007 *Phys. Rev. B* **75** 184429
[30] Y P Ivanov, M Vazquez and O Chubykalo-Fesenko 2013 *J. Phys.* D: Appl. Phys. **46** 485001